

RSC Advances



This is an *Accepted Manuscript*, which has been through the Royal Society of Chemistry peer review process and has been accepted for publication.

Accepted Manuscripts are published online shortly after acceptance, before technical editing, formatting and proof reading. Using this free service, authors can make their results available to the community, in citable form, before we publish the edited article. This *Accepted Manuscript* will be replaced by the edited, formatted and paginated article as soon as this is available.

You can find more information about *Accepted Manuscripts* in the [Information for Authors](#).

Please note that technical editing may introduce minor changes to the text and/or graphics, which may alter content. The journal's standard [Terms & Conditions](#) and the [Ethical guidelines](#) still apply. In no event shall the Royal Society of Chemistry be held responsible for any errors or omissions in this *Accepted Manuscript* or any consequences arising from the use of any information it contains.

Monitoring crosslinking inhomogeneities in ethylene vinyl acetate photovoltaic encapsulants using Raman microscopy

Abhishek Sanoria^a, Daniel Ulbricht^b, Tobias Schuster^a, Robert Brüll^{a}*

^a **Fraunhofer Institute for Structural Durability and System Reliability**, Division Plastics, Group Material Analytics, Schlossgartenstrasse 6, 64289 Darmstadt, Germany

^b **Evonik Industries AG**, Rodenbacher Chaussee 4, 63457 Hanau-Wolfgang

*Corresponding author: Dr. Robert Brüll, robert.bruell@lbf.fraunhofer.de

Abstract

Crosslinked ethylene vinyl acetate (EVA) resin is the preferred material for encapsulation of photovoltaic (PV) modules. Yet, profiling the spatial homogeneity of crosslinking in a quantitative and non-destructive way still remains a challenge. With the aid of reference techniques and using carefully prepared and well characterized model systems we have developed a protocol for Raman microscopy, which can determine the degree of crosslinking in EVA sheets in a quantitative manner. The new method has then been applied to characterize inhomogeneities with regard to crosslinking in EVA samples on various length scales, going down to a few μm . Finally, this method has been used to study crosslinking in EVA/glass laminates. The applicability and limitations of measuring crosslinking under glass was probed.

Keywords

Raman Microscopy, crosslinking, ethylene vinyl acetate, photovoltaic modules.

Introduction

Photovoltaic (PV) modules typically consist of two symmetric layers of solar cells which are encapsulated between two protective films. The latter are in turn mechanically stabilized on the rear side by a ‘backsheet’ and on the front side by glass or a suitable polymer film. The encapsulant material primarily protects the solar cells against weathering conditions and also provides mechanical stability. It also allows for sufficient isolation of the electrical components to maximize the optical coupling between the solar cells and the incident solar irradiation ^[1]. Therefore, the mechanical behavior of the encapsulant is one of the major properties defining the type of encapsulant used ^[2-4]. The setup of a PV module is shown in Figure 1.

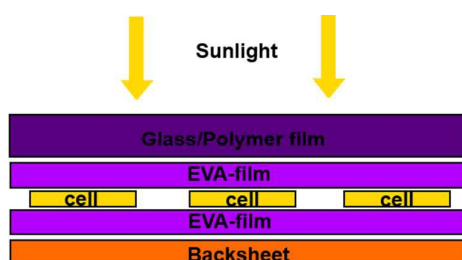


Figure1: Setup of a PV module

As seen from the figure, the encapsulant material surrounds the PV cells and provides a rigid support structure. Essential criteria for the encapsulant are high light transmission rates, low sensitivity to degradation by light, good adhesion to the backsheet, solar cell and front glass. ^[3]. To compensate the buildup of mechanical forces as a result of temperature fluctuation or mechanical load (e.g. wind), the encapsulant must have elastomeric properties. Materials used as encapsulant are silicone resin, polyvinyl butyral resin and transparent encapsulants

including thermoplastics such as EVA and ionomers ^[5-8]. EVA, the most commonly used material, is a co-polymer of vinyl acetate and ethylene. Ionomers are copolymers of ethylene and methacrylic acid with a salt added to neutralize them. Ionomers can be used alone or in combination with ethylene 1-olefins comonomers. Encapsulant materials comprising both ionomers and ethylene 1-olefins have been previously reported ^[9, 10].

The technique of producing these encapsulant foils surrounding the cells is well known. In this procedure the additives and crosslinking agents are homogeneously mixed with the olefin-copolymer e.g., in an extruder, to give a polymer film. For the encapsulation of the solar cells, the PV module production is typically carried out in a vacuum lamination oven ^[11]. Therefore, the stacked setting of the PV-module is prepared first and then heated in the lamination oven. Thus, while the olefin-copolymer (e.g. EVA) is softening, the evacuation of the oven removes the air between the two encapsulant films, which is the most critical fabrication step, taking 4 to 6 minutes. An essential property of EVA is that it flows easily below its curing temperature attaining the shape of the surrounding module and making it suitable for such application ^[7, 12]. In the next step, pressure is exerted for several minutes via a membrane within the laminator, which leads to heat-sealing of the different layers within the PV-module and crosslinking of the encapsulant material. Typical lamination conditions favorable for production of PV-modules are temperatures between 140 °C and 155 °C with a holdup time between 12 min and 20 min. Maintaining a uniform profiles with regard to temperature and pressure is extremely important to ensure the production of high performance and air-bubble free modules ^[13].

Typically, a minute quantity of the cross linker (~ 0.7 wt. %) is used for crosslinking these laminates and being minute in quantity a thorough homogenization of the cross linker is required to ensure optimum properties of the laminates upon crosslinking ^[14]. Even minor fluctuations in the dispersion or in the processing conditions might have a large impact on the

crosslinking developing in the form of crosslinking inhomogeneities. These variations can manifest itself in the form of minor (local) and larger fluctuations depending on the dispersion of the cross linker and the presence of a temperature gradient along the module, which ultimately can affect the efficiency of the PV modules. Homogeneity in terms of crosslinking is important to ensure a long service lifetime and continuous power output.

Thus, studying the variation in crosslinking in PV laminates is of pivotal importance to ensure a high throughput system. Even small variations in crosslinking across the module due to variation in the crosslinking conditions/improper homogenization of the cross linker might have a great impact on the solar cell efficiency. Hence it is important to have a robust method to determine the crosslinking homogeneity in EVA modules, which can be used in an online mode for screening the crosslinking in modules non-destructively.

Raman spectroscopy, which is highly sensitive to minor variations in the morphology and chemical composition of polymers, has been widely used to analyze polymer blends, copolymers and polymer composites. The short spectral acquisition times and minimal sample preparation make it a predestined technique for online quality control and in-situ reaction monitoring ^[15, 16]. The coupling of a light microscope to the Raman instrument allows spatially high resolved profiling of morphological or chemical variations, which includes: blend compositions, functionalization of micro-polymer particles in colloids, identification of unknown materials in art works and quality control in pharmaceuticals^[15, 17-21]. The high spatial resolution and the depth of information retrieved has been widely applied for the analysis of confectioned polymer products, such as in multi layered films or fibers, where, due to the length scale, locating and identifying individual components is often impossible using other imaging techniques like infrared microscopy. Also changes in local composition and morphology can be monitored ^[22-26]. This has been successfully utilized to evaluate the

degradation of multilayered polymer back sheets in PV modules where the ageing behavior of each layer was analyzed individually using Raman microscopy^[20].

Using this sensitivity of Raman microscopy to variations in the polymer structure, the crosslinking of EVA encapsulant films will be analyzed and a method will be developed to quantitatively determine the percentage crosslinking in EVA samples. This model will then be applied to analyze local variations in crosslinking on various length scales in an inhomogeneously crosslinked EVA laminate. Finally, the applicability of the analytical method to EVA/glass laminates will be probed.

Materials

EVA encapsulant material

The EVA resin (Evatane 28-40 from Arkema, containing 28.3 mol % vinyl acetate, was conditioned with 1 wt. % *t*-butylperoxy (2-ethylhexyl)carbonate (TBPEHC from United Initiators; CAS: 34443-12-4) and 0.7 wt. % of the crosslinking booster triallyl isocyanurate (TAICROS[®] from Evonik; CAS: 1025-15-6), 0.3 wt. % of the adhesive promoter γ -Methacryloxypropyltrimethoxysilane (Dynasytan[®] Memo from Evonik; CAS: 2530-85-0) as well as stabilizers in typical amounts.

The EVA/additive mixture was extruded on a labextruder (Collin) having a 10 cm flat film extrusion die. The extrusion temperature was 77 °C- 80 °C, whereas the melt temperature was 88 °C. The EVA encapsulant film was wound up with a cooled chill-roll system. Lamination of the EVA encapsulant film (0.8 mm thick) was done between two Teflon sheets. According to the sample description below (Table 1), the lamination time was varied between zero and 20 min. The temperature setting was 150 °C and the pressure 0.7 kg/cm² (second step after applying vacuum).

Table 1: Sample description

Sample No.	Lamination time [min.]
V1	0
V2	3
V3	5
V4	8
V5	12
V6	15
V7	20
V8*	20
V9#	20

* Sample V8 was made with the same composition as above, but with 0.8 wt. % tert.-butylperoxy (2-ethylhexyl) carbonate, 0.5 wt. % of the crosslinking booster triallyl isocyanurate, and without any added adhesive promoter.

Sample V9 was made with the same composition as samples V1-V6. The lamination in this case was carried out between two sheets of quartz glass having a thickness of 1 mm.

Methods

Soxhlet extraction

The percentage crosslinking was determined using toluene and 1 g (M_1) of the polymer in a Soxhlet hull. The toluene dissolved the non-cross-linked material and flushed it out from the hull. The cross-linked polymer was then left in a swollen state in the hull and the residual

solvent was removed in vacuum at 100 °C. This left over material was then weighed (M_2) and crosslinking was determined. Three measurements were carried out per sample.

Differential scanning calorimetry

Circular samples with a diameter of 5 mm (ca. 10 mg) were cut out from the EVA laminates and were analyzed using a Mettler Toledo DSC 822e, which was calibrated with high purity indium and zinc standards. All samples were measured using a heating rate of 10 °C/min under an inert atmosphere of nitrogen between 25 and 230 °C, and the first heating cycle was used for analysis. Five measurements were carried out per sample.

FT-IR Spectroscopy

The measurements were recorded in ATR mode on a Nicolet 8700 spectrometer equipped with a MCT-A detector. Three measurements were carried out per sample at a spectral resolution of 4 cm^{-1} . A background spectrum was recorded before each sample analysis, and 16 scans were carried out per measurement.

Raman Spectroscopy

Raman measurements were carried out using a WITec alpha 500 spectroscopy system and analyzed using the WITec Project Four software for data evaluation. For measurements on samples, a 50× (NA 0.8, spot diameter: 811 nm) microscope objective was used to focus the laser beam and to collect the scattered light. Laser radiation having a wavelength of 532 nm with a power of about 50 mW was employed as an excitation source. The scattered light was analyzed in a 600 mm^{-1} grating spectrometer at a spectral resolution of 1 cm^{-1} . After localizing the sample and focusing manually with the microscope, the laser spot was positioned to accumulate a single spectrum with an acquisition time of 2 s, and 10 accumulations were carried out per measurement. Each spectrum was smoothed using the Savitzky-Golay method and background subtracted. Ten independent measurements at

random positions along the sample were carried out to obtain the spectra from each EVA foil. The crosslinking inhomogeneities were measured by analyzing an area of 3000 x 3000 μm at a step width of 7.5 μm obtaining 160000 spectra using a motorized scan stage. The high resolution measurement to analyze minor crosslinking inhomogeneities was carried out by measuring an area of 100 x 100 μm at a step width of 0.5 μm obtaining 40000 individual spectra using a piezo-driven scan stage. The measurement under the glass laminate was carried out by measuring an area of 5000 x 5000 μm at a resolution of 16 μm obtaining 90000 individual spectra.

Results and discussions:

The Raman spectrum of EVA in the range of the C-C stretching and the deformation vibrations of the CH_2 and CH_3 groups is shown below in Figure 2, and the fundamental modes of vibration are assigned in Table 2 ^[27, 28].

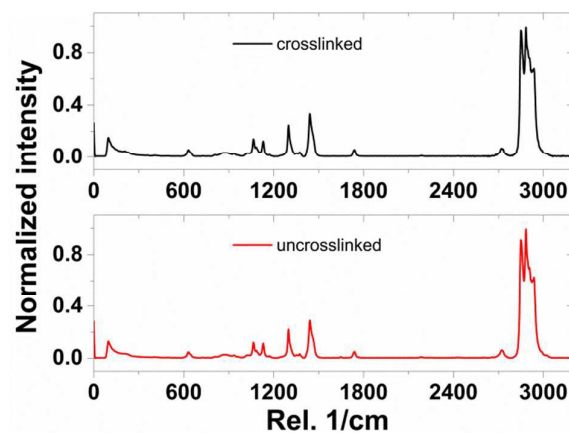


Figure 2: Raman spectrum of EVA

Table 2: Fundamental modes of vibration of the EVA spectrum

Wavenumber (cm^{-1})	Band assignment
---------------------------------	-----------------

2934, 2903, 2885, 2854 and 2725	Aliphatic C-H stretching (strong)
1740	C=O stretching of the acetate (mild)
1442, 1374, 1351 and 1300	C-H deformation (strong)
1200-1000	C-C stretching (strong)
640	C=O deformation (mild)

Upon crosslinking, pronounced changes in the form of additional bands are not observed, but significant changes in the region of the CH-stretching vibrations can be seen (Figure 3).

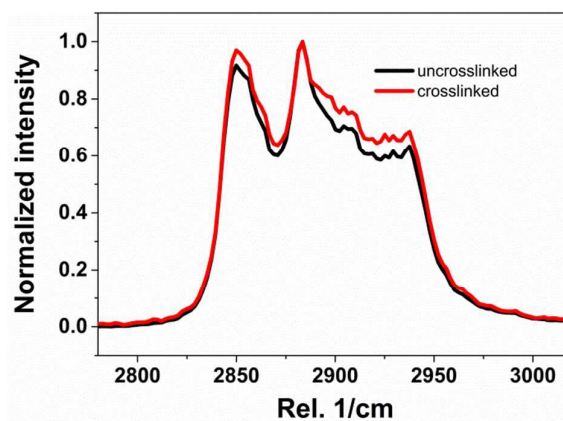


Figure 3: CH-stretching region of the Raman spectrum of EVA: spectral differences upon crosslinking

As seen from Figure 3, the intensity of the bands at 2934 and 2903 cm^{-1} is higher for the crosslinked sample compared to the uncrosslinked one. It has been previously reported that when normalizing the spectra to the highest intensity band at 2885 cm^{-1} , the relative intensity of the νCH_2 at 2934 and 2903 cm^{-1} increases upon crosslinking, while the relative intensity of νCH_3 at 2885 cm^{-1} decreases [27]. Crosslinking in EVA has been demonstrated to occur primarily via a radical reaction of the VA's terminal methyl groups, transforming these into methylene bridges, which leads to the spectral changes as reported [27, 29].

Seven samples as detailed previously, having different lamination time, were prepared (V1-V7), and the ratio I_{2934}/I_{2885} was plotted against the lamination time (Figure 4).

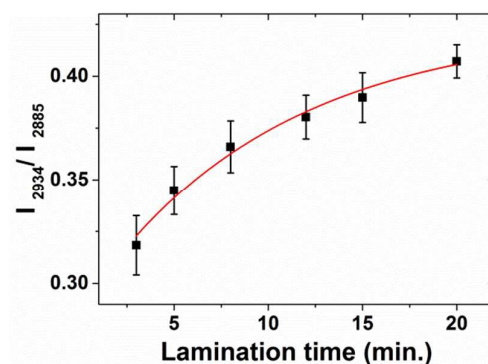


Figure 4: I_{2934}/I_{2885} variation with lamination time

The crosslinking starts exponentially and then converges towards a percolation value as seen in Figure 4, which is in accordance with the first order reaction mechanism proposed for the crosslinking of EVA [12].

To quantify the percentage of crosslinking using Raman spectroscopy, an interpretation of the band ratios has to be done with a method which can provide absolute values of crosslinking. This method can be used to assign band ratios to the percentage crosslinking and according to the calibration obtained, crosslinking in samples can be determined. DSC, FT-IR and Soxhlet extraction have been widely used to determine the degree of crosslinking in EVA laminates [27, 30-32]. Soxhlet extraction determines the percentage crosslinking as the ratio of the insoluble residue left in the hull to the initial mass of the sample. Figure 5 shows the percentage crosslinking as obtained from Soxhlet extraction (XC_{SE}) obtained for the sample series.

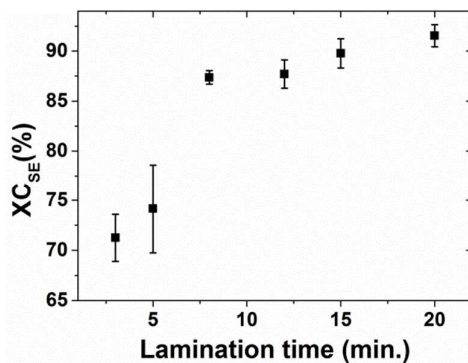


Figure 5: Percentage crosslinking determined through Soxhlet extraction (XC_{SE})

Even at low lamination times XC_{SE} is quite high, as can be recognized for the case of sample V2 which showed a crosslinking of $\sim 73\%$ after just 3 minutes of lamination. Chernev et al.^[27] reported a similar effect wherein Soxhlet extraction yields high XC_{SE} values even at low lamination times.

The percentage crosslinking can also be derived from DSC measurements (XC_{DSC}). The DSC trace of the first heating cycle of EVA is shown in Figure 6

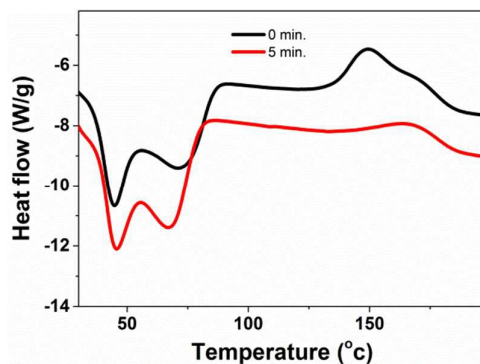


Figure 6: DSC curve showing the consumption of the crosslinker with reaction progress

An endothermic double peak showing the melting of the EVA resin can be recognized between 40 - 100 °C and an exothermic event resulting from the consumption of the crosslinker can be seen between 120 - 190 °C. The latter peak was used to calculate the percentage of crosslinking according to equation 1 by taking the enthalpy of the non-

crosslinked sample (ΔH_0) as a reference according to [33-37], where ΔH_s represents the enthalpy of the samples V2-V7 with a higher lamination time.

$$XC_{DSC} = \frac{\Delta H_0 - \Delta H_s}{\Delta H_0} \quad (1)$$

XC_{DSC} as a function of the lamination time is shown in Figure 7.

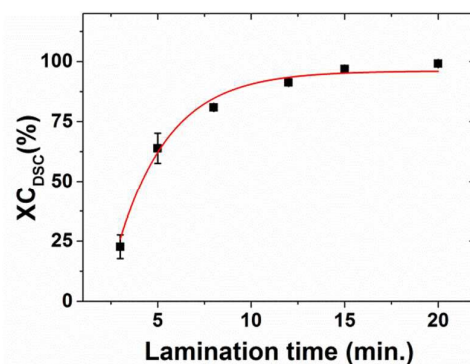


Figure 7: XC_{DSC} with the standard deviation calculated from three independent measurements.

The values obtained from the DSC also show a clear first order trend.

Infrared (IR) spectroscopy has also been used previously to determine the percentage crosslinking in EVA laminates [27]. IR measurements were carried out on the laminates to determine the crosslinking content. Yet, the samples were too thick to be analyzed in transmission and hence were measured in Attenuated Total Reflectance (ATR) mode. The spectra are shown in Figure.

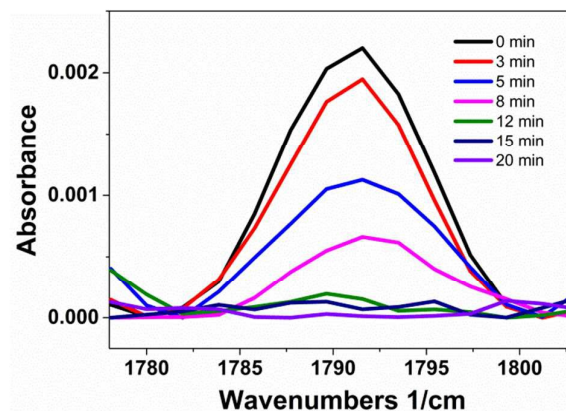


Figure 8: Intensity of the band at 1791 cm^{-1} in ATR measurements, attributed to the crosslinker.

An absorption at 1791 cm^{-1} can be recognized in the spectra, which gradually loses intensity at higher lamination time and finally vanishes at a lamination time > 8 minutes. This band can be attributed to the peroxy carbonate C=O stretching vibration ^[38] of the crosslinker. The amount of crosslinker is considered to be remaining in trace amounts and is not detectable beyond this stage, owing to the rapid consumption in the first order kinetics. Additionally, the ATR spectra have been shown to be affected by experimental parameters such as the applied pressure, the surface area being measured and the change in the refractive index with the penetration depth ^[39]. The non-detection of the crosslinker by FT-IR measurements owing to its rapid consumption and the limitations of the ATR method with regard to quantification as detailed previously made it unsuitable for drawing out any correlation between the percentage crosslinking and the reaction progress. Hence, the feasibility of studying the crosslinking behavior was compared between the values obtained for XC_{DSC} and XC_{SE} shown in Figure 9.

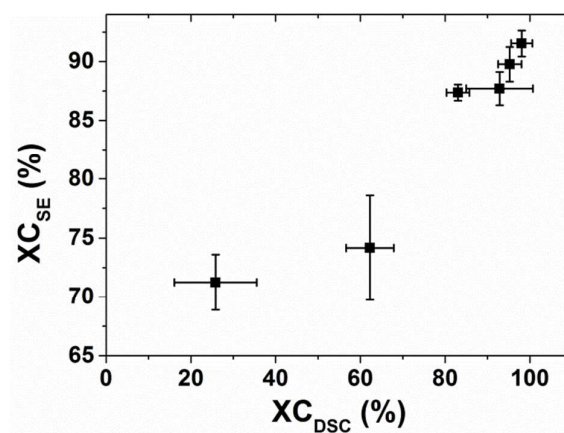


Figure 9: XC_{DSC} versus XC_{SE}

From Figure 9 it can be inferred that for lower lamination time, the Soxhlet method over predicts the value of crosslinking, while the DSC approach under predicts the crosslinking at higher lamination times. This can be explained as the Soxhlet method measures the fraction of non extractable polymer chains and even very few bonds formed during crosslinking may render a chain as non extractable. The gel content does not discriminate between single and multiple crosslinked chains ^[29] and as a consequence, a high value of gel content is observed even at low lamination times.

The under prediction in DSC can be explained by insufficient sensitivity of the thermocouple for the exothermic event at minute concentrations of crosslinker. On a broader perspective, techniques such as DSC and FT-IR spectroscopy which rely on determining the percentage crosslinking through the amount of residual crosslinker are limited by the sensitivity to the low amount of the crosslinker present in samples with higher lamination time. Hence, XC for sample V7 as obtained through Soxhlet extraction was used to translate the band ratios obtained from Raman measurements into absolute values of crosslinking.

A linear translation from the band ratio ν_{CH_3} / ν_{CH_2} into the percentage crosslinking can be postulated as

$$XC_R = M * (I_{2934}/I_{2885}) + C \quad (2)$$

Where 'XC_R' denotes the percentage crosslinking obtained from Raman measurements, M denotes the slope of the straight line translation with C being the intercept. To determine the values of the unknown parameters M and C two boundary conditions are needed. These were selected as firstly being the band ratio 2934 cm⁻¹/2885 cm⁻¹ of an uncrosslinked sample, V₀, determined to be 0.306. The second point of consideration was taken as XC_{SE} for the sample V7, determined to be 91.5 % and having a band ratio 2934 cm⁻¹/2885 cm⁻¹ of 0.407. Using these two end points, eq. (2) was solved for the unknown parameters M and C as shown as below.

$$\text{Point 1: } 0 = M * 0.306 + C$$

$$\text{Point 2: } 91.5 = M * 0.407 + C$$

By solving these equations the correlation obtained between XC_R and the band ratio is

$$XC_R = 906.2 I_{BR} - 277.3 \quad (3)$$

Using this correlation between XC_R and I_{BR}, the band ratios in Figure were translated into percentage crosslinking and plotted against the lamination time (Figure 10).

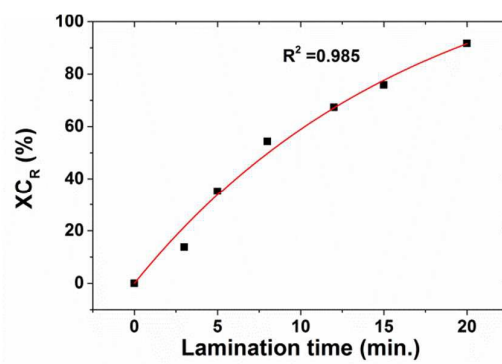


Figure 10: Raman degree of crosslinking determined using equation (3)

As seen from Figure 10, a good correlation to the first order fitting of the crosslinking reaction mechanism of EVA proposed by Schröder et. al ^[12] can be observed. This further suggests that the method developed to translate the band ratios into absolute crosslinking numbers based on the percentage crosslinking obtained through Soxhlet extraction can be accurately applied to determine the percentage of crosslinking in a quantitative manner when an EVA resin with similar VA content was crosslinked under identical conditions.

A crucial question when developing structure↔property relationships for films is how the degree of crosslinking is spatially distributed i.e., identifying inhomogeneities. To provoke inhomogeneities, sample V8 was crosslinked by using a lower amount of both the crosslinker and the crosslinking promoter. Raman microscopy was carried out over a selected area and the spectra collected over the entire region were analyzed. The intensity of the CH₃ stretching region was calculated and plotted for each spectrum obtained to identify the presence of such inhomogeneities (Figure 11 a).

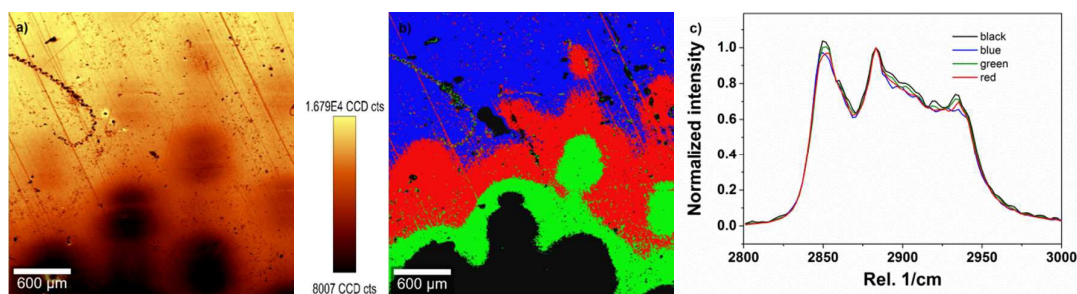


Figure 11: a) Intensity map of the CH₃ stretching region from 2800-3000 cm⁻¹ b) Segregation of Raman spectra obtained based on spectral differences c) Raman spectra representative for the average in the individual clusters

The intensity map of the CH₃ stretching region in Figure 11 a shows a clear variation in intensity, which suggests possible fluctuations in crosslinking over the area. Four distinct clusters were obtained by spectral segregation (Figure 11 b) showing differences in the intensity of the bands in the CH₃ stretching region (Figure 11 c). From the spectra it can be

observed that the νCH_2 band at 2934 cm^{-1} and the νCH_3 band at 2885 cm^{-1} show a large variation in intensity within the clusters obtained. These spectral differences were analyzed and the average band ratio I_{2934}/I_{2885} was calculated for each of the four clusters. Using the calibration model developed earlier these band ratios were then translated into XC_R values. The blue region was seen to be uncrosslinked as the band at 2934 cm^{-1} was very low in intensity compared to the other regions. The other three regions, namely the red, green and the black area show an average degree of crosslinking of 27, 54.5 and 94.2 % respectively. An explanation for this would be an inhomogeneous distribution of the crosslinker, augmented by the effect of an insufficient amount of crosslinking promoter, which ultimately lead to inhomogeneity in crosslinking across the sample.

The same sample was also investigated with regard to locally more confined inhomogeneities, in the order of a few μm . An area $100 \times 100\ \mu\text{m}$ was analyzed and the spectra were collected every $0.5\ \mu\text{m}$. The data generated were segregated and clustered as described above. The intensity map of the CH_3 stretching region in this area is shown in Figure 12 a.

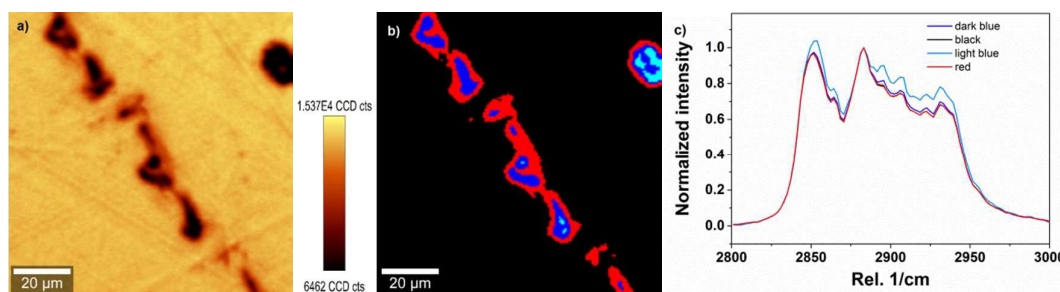


Figure 12: a) Intensity map of the CH_3 stretching region from $2800\text{-}3000\text{ cm}^{-1}$ b) Segregation of Raman spectra obtained based on spectral differences c) Raman spectra representative for the average in the individual clusters

The CH_3 stretching region shows a variation in intensity in the form of small inclusions/spots as seen in Figure 12 a. The spectral dataset showing the clusters based on spectral differences is shown in Figure 12 b and the average spectrum obtained for each of these clusters is shown

in Figure 12 c. Again, clear differences in crosslinking are observable with the intensity of the νCH_2 band at 2934 cm^{-1} and the νCH_3 band at 2885 cm^{-1} . The νCH_2 band shows an increase in intensity in the innermost region of the inclusion compared to the region where the spots are not present. The band ratio I_{2934}/I_{2885} was calculated and translated into percentage crosslinking based on the model proposed previously. The black, red, dark blue and light blue regions were found to have an average crosslinking of 16.2 %, 17.1 %, 30.6 % and 106.9 %. A tiny region shown in light blue can be recognized, which was highly crosslinked compared to the surrounding polymer. The occurrence of such pronounced inhomogeneities can be explained as the result of a local maximum in crosslinker concentration, causing this area area to crosslink intensely.

After developing a method to study inhomogeneities in crosslinking on different length scales using model systems prepared between Teflon sheets, it is essential to transfer this model to glass-laminates. This was probed using sample V9. A major advantage of Raman microscopy is the fact that measurements can be carried out without destroying the glass laminates by measuring through the glass. Transparent silicate materials like glass do not generate intense Raman signatures, hence the Raman scattering is unfazed by the presence of a glass layer on the measuring surface^[40-42]. The spectral dataset obtained upon mapping of V9 was analyzed as previously, and the intensity of the CH_3 stretching region was plotted to determine local inhomogeneities in crosslinking across the sample (Figure 13 a).

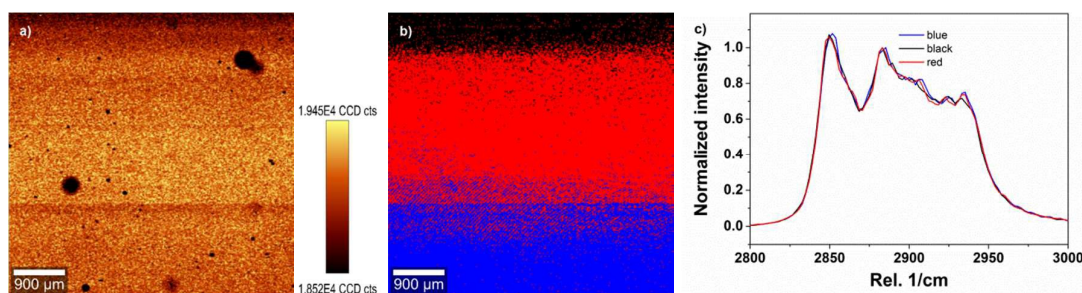


Figure 13: a) Intensity map of the CH₃ stretching region from 2800-3000 cm⁻¹ b) Segregation of Raman spectra obtained based on spectral differences c) Raman spectra representative for the average in the individual clusters

The intensity of the CH₃ stretching region is inhomogeneously distributed suggesting differences with regard to crosslinking across the sample. The spectral dataset was then clustered (Figure 13 c) and three distinct regions could be distinguished based on differences in the spectra as shown in Figure 13 b. The clustered regions seen in this case showed three distinct layers, whereas the distribution seen previously for sample V8 was more irregular. The XC_R in the above three distinct black, red and blue clusters was calculated and found to be 121.8 %, 248 % and 235.2 %, respectively. This implies that the major difference in crosslinking is present along the top edge of the sample, whereas the other two regions show almost similar values of XC_R . Such broad inhomogeneities might result from differences in the cooling/heating patterns of the glass laminate being predominant at the sample edge.

Surprisingly, the values of crosslinking are considerably higher than those of sample V7. These differences were assessed by analyzing the spectra of a highly crosslinked region measured under the glass laminate. An overlay of the spectra of sample V7 and the spectrum of an uncrosslinked material is shown in Figure 14.

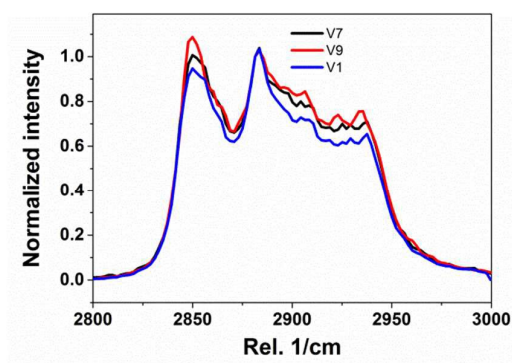


Figure 14: Comparison of crosslinking under glass to EVA sheets laminated under Teflon

Figure 14 clearly confirms a higher intensity for the bands at 2934 and 2903 cm^{-1} in the glass laminate compared to samples V7 and V1. The increase in the intensity of these bands reveals the consumption of more CH_3 units in the glass laminate, suggesting the formation of CH_2 bridges for multiple crosslinking. This can be due to the fact that the crosslinking of sample V7 was carried out under Teflon sheets, which leads to differences compared to the process carried out under glass: In the first case the crosslinking process is inhibited by a sudden quenching of the samples as the sheets are removed. However, crosslinking under glass involves annealing of the laminates as the samples are removed from the oven, wherein multiple crosslinks are still forming in the material as it cools down slowly, insulated due to the low thermal conductivity ($\sim 0.9 \text{ W/m K}$)^[43] of the glass covering. The glass covering also does not allow the trapped thermal energy to be radiated out easily being opaque to IR radiation^[44]. Convective heat transfer is also much lower compared to the samples produced between Teflon sheets which can freely lose thermal energy to the surrounding air once the sheets are removed. This explains the higher amount of crosslinking as observed in the glass laminate.

Conclusions

Assessing the degree of crosslinking, XC, of ethylene vinyl acetate resin in photovoltaic modules remains a challenge, which has a great impact on the cell efficiency. Various techniques such as DSC, FT-IR and Soxhlet extraction have been used for this purpose. All these approaches lack spatial resolution per se, as they are limited to bulk differences in XC, whereas local inhomogeneities are averaged out. In the present study a method based on Raman microscopy has been developed to study local variations in crosslinking in PV modules and quantify these. The signal intensity of the respective bands in the spectra reflects the transformation of methyl groups into methylene bridges as a consequence of crosslinking, and thus the conversion. Yet, this information is of relative nature, and to translate it into absolute values, a calibration of the Raman bands was carried out using an uncrosslinked sample and the results from Soxhlet extraction for a highly crosslinked sample as reference. The method developed has then been applied to characterize inhomogeneities with regard to crosslinking in EVA films prepared between Teflon sheets on various length scales, ranging down to a few μm . As Raman microscopy is indifferent to measuring under glass, the developed method has then been applied to study crosslinking inhomogeneities in EVA/glass laminates. In this case the quantification of crosslinking yielded significantly higher values for XC_R compared to the model films prepared between Teflon sheets. Raman microscopy being the only technique sensitive to measuring multiple crosslinks in the samples delivers a higher XC value for this system compared to the system without the glass. This observation has been attributed to differences in the cooling pattern of the glass system, causing the formation of multiple crosslinks. This is a very important conclusion, as it clearly demonstrates the limitations for transferring results from a model system to the real process.

References

- [1] L. K. J in *Encapsulant Material Requirements for Photovoltaic Modules*, Vol. 220, AMERICAN CHEMICAL SOCIETY, **1983**, pp.367-385.
- [2] N. G. Dhere, N. R. Raravikar *Solar Energy Materials and Solar Cells*. **2001**, 67, 363-367.
- [3] A. W. Czanderna, F. J. Pern *Solar Energy Materials and Solar Cells*. **1996**, 43, 101-181.
- [4] F. J. Pern, S. H. Glick, A. W. Czanderna *Renewable Energy*. **1996**, 8, 367-370.
- [5] R. M. Patel, S. Wu, M. T. Bernius, M. Esseghir, R. L. Mcgee, M. H. Mazor, J. Naumovitz *US patent: 8581094 B2*, **2008**.
- [6] A. Roos, M. Herrmann, R. Kalkofen, S. Kelbch, H. J. Frommont, G. Bergmann, R. Tappe *US patent: 20120190766 A1*, **2012**.
- [7] M. D. Kempe, G. J. Jorgensen, K. M. Terwilliger, T. J. McMahon, C. E. Kennedy, T. T. Borek *Solar Energy Materials and Solar Cells*. **2007**, 91, 315-329.
- [8] J. Schlothauer, S. Jungwirth, M. Köhl, B. Röder *Solar Energy Materials and Solar Cells*. **2012**, 102, 75-85.
- [9] J. I. Hanoka *WO Patent: 1999017379 B1*, **2001**.
- [10] J. I. Hanoka, P. P. Klemchuk *US patent: 6187448 B1*, **2001**.
- [11] N. Damm *EP patent: 2457728 B1*, **2013**.
- [12] S. Kajari-Schröder, U. Eitner, C. Oprisoni, T. Alshuth, M. Köntges, R. Brendel *EU PVSEC Proceedings*. **2010**, 4039-4043.
- [13] R. F. M. Lange, Y. Luo, R. Polo, J. Zahnd *Progress in Photovoltaics: Research and Applications*. **2011**, 19, 127-133.
- [14] F. J. Pern *US patent: 6093757 A*, **2000**.
- [15] A. Sanoria, T. Schuster, R. Brull *Analytical Methods*. **2015**, 7, 5245-5253.
- [16] O. Svensson, M. Josefson, F. W. Langkilde *Chemometrics and Intelligent Laboratory Systems*. **1999**, 49, 49-66.
- [17] S. Bhaskar, C. T. Gibson, M. Yoshida, H. Nandivada, X. Deng, N. H. Voelcker, J. Lahann *Small*. **2011**, 7, 812-819.
- [18] L. Markwort, B. Kip *J Appl Polym Sci*. **1996**, 61, 231-254.
- [19] M. D. Schaeberle, C. G. Karakatsanis, C. J. Lau, P. J. Treado *Analytical Chemistry*. **1995**, 67, 4316-4321.
- [20] C.-C. Lin, P. J. Krommenhoek, S. S. Watson, X. Gu *Solar Energy Materials and Solar Cells*. **2016**, 144, 289-299.
- [21] G. Turrell, J. Corset, Raman microscopy: developments and applications, Academic Press, **1996**.
- [22] R. J. Young, R. J. Day *British Polymer Journal*. **1989**, 21, 17-21.
- [23] A. Garton, D. N. Batchelder, C. Cheng *Applied spectroscopy*. **1993**, 47, 922-927.
- [24] R. Appel, W. Xu, T. W. Zerda, Z. Hu *Macromolecules*. **1998**, 31, 5071-5074.
- [25] J. Breitenbach, W. Schrof, J. Neumann *Pharmaceutical research*. **1999**, 16, 1109-1113.
- [26] A. S. Nielsen, D. Batchelder, R. Pyrz *Polymer*. **2002**, 43, 2671-2676.
- [27] B. S. Chernev, C. Hirschl, G. C. Eder *Applied Spectroscopy*. **2013**, 67, 1296-1301.
- [28] M. Shimoyama, H. Maeda, K. Matsukawa, H. Inoue, T. Ninomiya, Y. Ozaki *Vibrational spectroscopy*. **1997**, 14, 253-259.
- [29] C. Hirschl, M. Biebl-Rydlo, M. DeBiasio, W. Mühleisen, L. Neumaier, W. Scherf, G. Oreski, G. Eder, B. Chernev, W. Schwab, M. Kraft *Solar Energy Materials and Solar Cells*. **2013**, 116, 203-218.
- [30] F. Li, W. Zhu, X. Zhang, C. Zhao, M. Xu *J Appl Polym Sci*. **1999**, 71, 1063-1070.
- [31] H.-Y. Li, L.-E. Perret-Aebi, R. Théron, C. Ballif, Y. Luo, R. F. M. Lange *Progress in Photovoltaics: Research and Applications*. **2013**, 21, 187-194.
- [32] M. K. Weiss *Open Journal of Renewable Energy and Sustainable Development*. **2014**, 1.
- [33] W. Stark, M. Jaunich *Polym Test*. **2011**, 30, 236-242.
- [34] O. Bianchi, R. V. B. Oliveira, R. Fiorio, J. D. N. Martins, A. J. Zattera, L. B. Canto *Polym Test*. **2008**, 27, 722-729.

- [35] P. Klemchuk, M. Ezrin, G. Lavigne, W. Holley, J. Galica, S. Agro *Polymer Degradation and Stability*. **1997**, 55, 347-365.
- [36] M. Schubnell *Photovoltaics International*. **2010**, 7, 131-137.
- [37] W. Stark, M. Jaunich, W. Bohmeyer, K. Lange *Polym Test*. **2012**, 31, 904-908.
- [38] G. Socrates, *Infrared and Raman characteristic group frequencies: tables and charts*, John Wiley & Sons, **2004**.
- [39] T. M. Theophanides, *Infrared Spectroscopy - Materials Science, Engineering and Technology*, InTech, **2012**.
- [40] S. Ekins, S. Sasic, *Pharmaceutical applications of Raman spectroscopy*, John Wiley & Sons, **2008**.
- [41] E. Li-Chan, J. Chalmers, P. Griffiths, *Applications of vibrational spectroscopy in Food Science*, John Wiley & Sons, **2011**.
- [42] M. de la Guardia, S. Garrigues, *Handbook of green analytical chemistry*, John Wiley & Sons, **2012**.
- [43] O. A. Sergeev, A. G. Shashkov, A. S. Umanskii *Journal of Engineering Physics*. **1982**, 43, 1375-1383.
- [44] R. Kitamura, L. Pilon, M. Jonasz *Applied optics*. **2007**, 46, 8118-8133.